




Optical nonreciprocity and nonreciprocal photonic devices with directional four-wave mixing effect

TAO SHUI,^{1,6} WEN-XING YANG,^{1,7}  MU-TIAN CHENG,² AND RAY-KUANG LEE^{3,4,5} 

¹*School of Physics and Optoelectronic Engineering, Yangtze University, Jingzhou, Hubei, 434023, China*

²*School of Electric Engineering and Information, Anhui University of Technology, Ma'anshan, Anhui 243002, China*

³*Institute of Photonics Technologies, National Tsing Hua University, Hsinchu 300, Taiwan*

⁴*Center for Quantum Technology, Hsinchu 30013, Taiwan*

⁵*Physics Division, National Center for Theoretical Sciences, Taipei 10617, Taiwan*

⁶*ahushuitao@126.com*

⁷*wenxingyang2@126.com*

Abstract: A scheme for magnetic-free optical nonreciprocity in an ensemble of four-level cold atoms is proposed by exploiting the directional four-wave mixing effect. Using experimentally achievable parameters, the nonreciprocal optical responses of the system can be observed and the conversion on nonreciprocal transmission and nonreciprocal phase shift can be implemented. These nonreciprocal phenomena originate from the directional phase matching, which breaks the time-reversal symmetry and dynamic reciprocity of the cold atomic system. Moreover, by embedding the cold atoms into a Mach-Zehnder interferometer and choosing proper parameters, a two-port optical isolator with an isolation ratio of 79.70 dB and an insertion loss of 0.35 dB and a four-port optical circulator with a fidelity of 0.9985 and a photon survival probability of 0.9278 can be realized, which shows the high performance of isolation and circulation. The proposal may enable a new class of optically controllable cavity-free nonreciprocal devices in optical signal processing at the low light level.

© 2022 Optica Publishing Group under the terms of the [Optica Open Access Publishing Agreement](#)

1. Introduction

In the past several decades, the study of optical nonreciprocity has been one of the hottest spots in the field of optics due to its significant applications in photonic networks and optical information processing [1]. Note that the constraint of the Lorentz reciprocal theorem makes it impossible to generate an optical nonreciprocal response in a nonmagnetic, linear and time-invariant medium [2]. Accordingly, the way to circumvent Lorentz reciprocity and realize optical nonreciprocity relies on time-reversal symmetry breaking of an optical system. A traditional approach for creating optical nonreciprocity is to use the magneto-optical effect, i.e., by applying an external magnetic bias on magneto-optical material [3,4]. Despite its commercial success, there are some problems such as material's incompatibility with the mature complementary metal-oxide semiconductor (CMOS) technique and significant loss in optical domain. For this reason, significant efforts have been made to develop magnetic-free optical nonreciprocity via adopting different linear modulation methods, such as travelling-wave modulation [5–7], direct photonic transition [8,9], synthetic angular momentum [10–12], optomechanical interaction [13–18], directional spin-orbit coupling [19,20], non-Hermiticity [21,22]. With these methods, numerous complete nonreciprocal photonic devices including optical isolators [5,6,11–13,18–20], circulators [15,17] and directional amplifiers [9,17], have been theoretically proposed and experimentally realized. Although these concepts are elegant, most of the reported schemes rely on complex structures

and special modulation technologies. In contrast to linear magnetic-free optical nonreciprocity, some attention has been devoted to break Lorentz reciprocity via introducing optical nonlinearity. For instance, magnetic-free optical nonreciprocity and nonreciprocal photonic devices have been demonstrated with Kerr nonlinearities [23,24], thermo-optic effect [25], stimulated Brillouin scattering [26], parametric amplification [27,28], etc [29,30]. However, most nonlinearity-based schemes rely on optical microcavities with high Q factor, which require complicated fabricated process. Therefore, realizing magnetic-free optical nonreciprocity in a simple and efficient optical system still remains to be explored.

On the other hand, based on electromagnetically induced transparency (EIT) [31,32], the atomic ensemble provides a promising platform for all-optical control of photon transport [33]. Up to now, a host of breakthroughs have been made such as electromagnetically induced grating [34,35], subluminal and superluminal propagation [36,37] and non-Hermitian systems [38,39]. Recently, magnetic-free optical nonreciprocity has also been achieved via combining EIT and asymmetric Doppler shifts in moving atomic Bragg lattices [40–43] and hot atomic gases [44–46]. Such proposals have obvious advantages of all-optical controllable and reconfigurable capabilities, which have been used for realizing cavity-free optical isolators and circulators [47–49]. It is well known that EIT in an ensemble of cold atoms can greatly enhance nonlinear susceptibility without significant absorption losses [50], which have found applications in nonlinear optics of weak light, such as giant Kerr nonlinearity [51,52], enhanced four-wave mixing (FWM) [53–55], cross-phase modulation [56] and so on. Motivated by previous investigations for microcavity-based optical nonreciprocity [23–27,29,30], one question is evoked: Can we achieve magnetic-free optical nonreciprocity and realize cavity-free nonreciprocal photonic devices with enhanced FWM effect in a cold atomic medium?

To answer this question, a scheme is proposed in this paper to achieve nonreciprocal optical behaviors via directional FWM effect in a cold atomic ensemble with four-level configuration. It is demonstrated that the optical depth and driving detuning play important roles in the manipulation of nonreciprocal optical responses of the atomic medium. For suitable values of the parameters, the optimal nonreciprocal transmission and nonreciprocal phase shift with high transmission can be achieved. Different from the mechanisms of the controllable optical nonreciprocity in previous investigations [40–49], the realization of optical nonreciprocity originates from the directional phase matching controlled by the propagation direction of the probe field. Subsequently, by inserting the cold atomic medium into a Mach-Zehnder interferometer (MZI), a reconfigurable nonreciprocal device with alternative functions as a isolator or a circulator is designed and analyzed based on the nonreciprocal phase shift with high transmission. It is found that the isolation ratio and insertion loss of the optical isolator can reach approximately 79.70 and 0.35 dB, respectively, and the optical circulator has a fidelity of 0.9985 and a photon survival probability of 0.9278, which are greatly improved compared with the performance indices in the previous schemes [47–49]. By now, the proposed question is settled satisfactorily. Magnetic-free optical nonreciprocity and cavity-free nonreciprocal photonic devices can be realized with enhanced FWM effect in a cold atomic medium. Our proposal can provide an avenue for the manipulation of magnetic-free optical nonreciprocity and a possibility of cavity-free nonreciprocal photonic devices at low light level.

The paper is organized as follows. In Sec. 2., we introduce the theoretical model and show the expressions of the forward and backward probe fields. In Sec. 3., we discuss the nonreciprocal optical responses and its potential applications in optical isolator and circulator. Our conclusions are given in Sec. 4.

2. Models and equations

The schematic of the proposed optical nonreciprocity is depicted in Fig. 1(a). An ensemble of cold ^{87}Rb atoms is driven by a coupling field and a driving field, both of which propagate at a

small angle of 1° with respect to $+z$ axis. Here, a four-level atomic system with two excited states ($|3\rangle$ and $|4\rangle$) and two ground states ($|1\rangle$ and $|2\rangle$) is considered, as illustrated in Figs. 1(b) and 1(c). The designated states of ^{87}Rb atoms are chosen as follows: $|1\rangle = |5^2S_{1/2}, F = 1, m_F = 0\rangle$, $|2\rangle = |5^2S_{1/2}, F = 2, m_F = 0\rangle$, $|3\rangle = |5^2P_{1/2}, F' = 2, m'_F = -1\rangle$ and $|4\rangle = |5^2P_{1/2}, F' = 2, m'_F = 1\rangle$. A weak probe field $\Omega_p^{f,b}$ is applied to the transition $|3\rangle \leftrightarrow |1\rangle$, while the transitions $|3\rangle \leftrightarrow |2\rangle$ and $|4\rangle \leftrightarrow |2\rangle$ are driven by a coupling field Ω_c and a driving field Ω_d , respectively. According to the transition selection rules [57], the probe and coupling fields are left circularly polarized (σ^-) while the driving field is right circularly polarized (σ^+). For the forward-propagation case, the weak probe field (denoted by Ω_p^f) propagates through the cold atomic medium in the forward ($+z$) direction. In this situation, the phase-matching condition of FWM can be satisfied, thereby leading to the generation of a forward σ^+ polarized FWM field Ω_m^f [see Fig. 1(b)]. In the backward-propagation case, the weak probe field (denoted by Ω_p^b) propagates along with the direction of $-z$ axis and there is no nonlinear frequency conversion owing to the lack of phase matching. As shown in Fig. 1(c), the FWM field does not exist when the probe field passes through the cold atomic medium in the backward direction. $\Omega_p^{f,b} = \mu_{31}E_p^{f,b}/2\hbar$, $\Omega_m^f = \mu_{41}E_m^f/2\hbar$, $\Omega_c = \mu_{32}E_c/2\hbar$, $\Omega_d = \mu_{42}E_d/2\hbar$ are half Rabi frequencies of the probe, FWM, coupling and driving fields with μ_{mn} ($m = 3, 4; n = 1, 2$) being the corresponding electric-dipole matrix element. In our proposal, all cold ^{87}Rb atoms are initially prepared at the specific Zeeman state $|5^2S_{1/2}, F = 1, m_F = 0\rangle$ ($|1\rangle$) via optical pumping and stimulated Raman adiabatic passage techniques [58]. Therefore, almost all ^{87}Rb atoms will remain in the ground state $|1\rangle$ (i.e., $\rho_{11} \approx 1$) for the forward and backward cases under the weak-field approximation, i.e., $\Omega_p^f, \Omega_m^f, \Omega_p^b \ll \Omega_c, \Omega_d$ [59]. Other hyperfine Zeeman states will not be involved since little atoms can be excited into states $|3\rangle$ and $|4\rangle$ to result in random spontaneous emission [60]. Therefore, one can solve the master equation with the perturbation approach and obtain the corresponding off-diagonal matrix elements in the steady state as

$$\rho_{31}^f = -\frac{D_p}{D}\Omega_p^f + \frac{\Omega_c\Omega_d^*}{D}\Omega_m^f, \quad (1)$$

$$\rho_{41}^f = -\frac{D_m}{D}\Omega_m^f + \frac{\Omega_c^*\Omega_d}{D}\Omega_p^f \quad (2)$$

for the forward case, and

$$\rho_{31}^b = -\frac{D_p}{D}\Omega_p^b \quad (3)$$

in the backward case [the formula derivations are given in Appendix], where $D_p = \Omega_d^2 - d_{21}d_{41}$, $D_m = \Omega_c^2 - d_{21}d_{31}$, $D = \Omega_d^2d_{31} + \Omega_c^2d_{41} - d_{21}d_{31}d_{41}$, $d_{21} = \Delta_2 + i\gamma_{21}$, $d_{31} = \Delta_1 + i\gamma_{31}$ and $d_{41} = \Delta_3 + i\gamma_{41}$. $\Delta_1 = \delta_p$, $\Delta_2 = \delta_p - \delta_c$ and $\Delta_3 = \delta_p - \delta_c + \delta_d$ represent the one-photon, two-photon and three-photon detunings, respectively. $\delta_p = \omega_p - \omega_{31}$, $\delta_c = \omega_c - \omega_{32}$ and $\delta_d = \omega_d - \omega_{42}$ are the detunings of the probe, coupling and driving fields, respectively. $2\gamma_{j1}$ ($j = 2, 3, 4$) is the decay rate of the coherence between the states $|j\rangle$ and $|1\rangle$. It is worth noting from Eqs. (1) and (3) that the off-diagonal matrix element ρ_{31} is composed of a direct-coupling term ($-D_p\Omega_p^f/D$) and a cross-coupling term ($\Omega_c\Omega_d^*\Omega_m^f/D$) in the forward direction, while it only contains a direct-coupling term ($-D_p\Omega_p^b/D$) in the backward direction. That is to say, the existence of the cross-coupling term depends on the propagation direction of the probe field, i.e., directional phase matching.

In the slowly varying amplitude approximation, one-dimensional (1D) Maxwell's equations can be expressed as

$$\frac{\partial \Omega_p^f(z, t)}{\partial z} + \frac{1}{c} \frac{\partial \Omega_p^f(z, t)}{\partial t} = i \frac{\alpha_p \gamma_{31}}{2L} \rho_{31}^f, \quad (4)$$

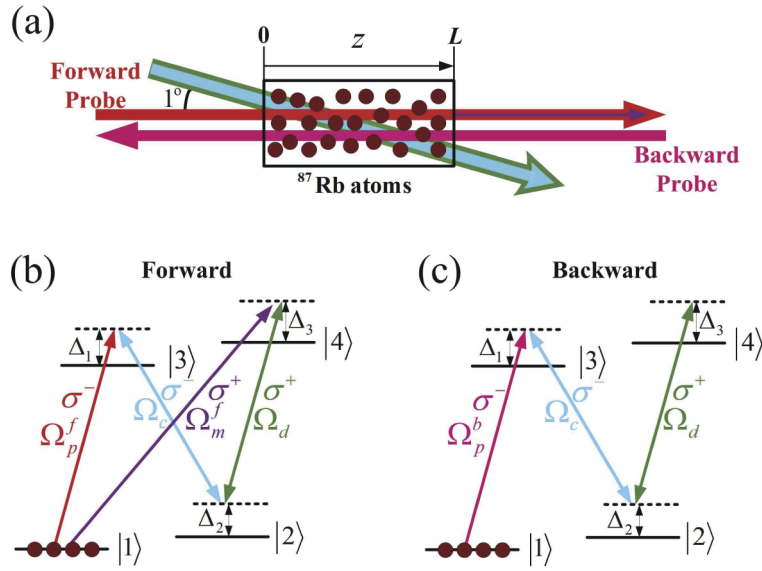


Fig. 1. (a) Schematic for realizing optical nonreciprocity with ensemble of cold ^{87}Rb atoms, which is driven by a coupling field and a driving field in the forward (+z) direction. Forward probe field suffers nonlinear frequency conversion in phase-matched four-wave mixing (FWM) process, whereas backward probe field goes through cold atoms with linear absorption and dispersion. Schematics of four-level atomic system interacting with (b) four applied fields ($\Omega_c, \Omega_d, \Omega_p^f, \Omega_m^f$) in forward direction and (c) three applied fields ($\Omega_c, \Omega_d, \Omega_p^b$) in backward direction.

$$\frac{\partial \Omega_m^f(z, t)}{\partial z} + \frac{1}{c} \frac{\partial \Omega_m^f(z, t)}{\partial t} = i \frac{\alpha_s \gamma_{41}}{2L} \rho_{41}^f \tag{5}$$

for the forward probe and FWM fields, and

$$\frac{\partial \Omega_p^b(z', t)}{\partial z'} + \frac{1}{c} \frac{\partial \Omega_p^b(z', t)}{\partial t} = i \frac{\alpha_p \gamma_{31}}{2L} \rho_{31}^b \tag{6}$$

for the backward probe field, where $z' = L - z$. $\alpha_p = N\sigma_{13}L$ ($\alpha_m = N\sigma_{14}L$) is the optical depth of the probe (FWM) transition, where N is the atomic density, σ_{13} (σ_{14}) is the atomic absorption cross section of the probe (FWM) transition, and L is the length of the atomic medium. Note that the optical depth can be effectively controlled by adjusting the density and length of the atomic medium. For simplicity, $\alpha_p = \alpha_s = \alpha$ and $\gamma_{31} = \gamma_{41} = \Gamma$ are selected. In our scheme, the intensities of the coupling and driving fields are spatially invariant as long as the probe and mixing fields are weak enough. Our interest is in the atomic response to the long probe and mixing pulses, such that $(1/c)\partial\Omega_i^j/\partial t = 0$ ($i = p, m; j = f, b$). After passing through the atomic medium with length L , the forward probe and FWM fields become

$$\Omega_p^f(\alpha) = \Omega_p^f(0)(A_{p+}^f e^{iK_+^f \alpha} - A_{p-}^f e^{iK_-^f \alpha}), \tag{7}$$

$$\Omega_m^f(\alpha) = \Omega_p^f(0)(B_{m+}^f e^{iK_+^f \alpha} + B_{m-}^f e^{iK_-^f \alpha}), \tag{8}$$

with

$$\begin{aligned} K_{\pm}^f &= \frac{(\pm\sqrt{G} - D_m - D_p)\Gamma}{4D}, \\ A_{p\pm}^f &= \frac{D_m - D_p \pm \sqrt{G}}{2\sqrt{G}}, \\ B_{m\pm}^f &= \pm \frac{G - (D_p - D_m)^2}{4\sqrt{G}\Omega_c\Omega_d^*}, \\ G &= (D_m - D_p)^2 + 4\Omega_c^2\Omega_d^2. \end{aligned}$$

In the meantime, the backward probe field becomes

$$\Omega_p^b(\alpha) = \Omega_p^b(0)e^{iK^b\alpha}, \quad (9)$$

with $K^b = -D_p\Gamma/2D$.

Here, we focus on the transmission characteristics of the forward and backward probe field, which is chosen as a signal. In terms of the scattering matrix [2], the probe field in Eqs. (7) and (9) can be recast into the following form

$$\begin{pmatrix} \Omega_p^b(\alpha) \\ \Omega_p^f(\alpha) \end{pmatrix} = \begin{bmatrix} 0 & \zeta_p^b e^{i\phi_p^b} \\ \zeta_p^f e^{i\phi_p^f} & 0 \end{bmatrix} \begin{pmatrix} \Omega_p^f(0) \\ \Omega_p^b(0) \end{pmatrix}, \quad (10)$$

where $\zeta_p^f e^{i\phi_p^f} = A_{p+}^f e^{iK_+^f\alpha} - A_{p-}^f e^{iK_-^f\alpha}$ and $\zeta_p^b e^{i\phi_p^b} = e^{iK^b\alpha}$. $\zeta_p^{f(b)}$ and $\phi_p^{f(b)}$ represent the transmission amplitude and phase shift of the forward (backward) probe field, respectively. It is obvious from the off-diagonal elements of the scattering matrix that the directional FWM can break Lorentz reciprocity and dynamic reciprocity, and thereby leading to nonreciprocal optical responses: nonreciprocal transmission (i.e., $\zeta_p^f \neq \zeta_p^b$) and nonreciprocal phase shift (i.e., $\phi_p^f \neq \phi_p^b$). Alternatively, Eq. (10) is applicable to describe photon transmission for both cases with simultaneously and separately inputting forward and backward probe fields.

3. Results and discussions

In this section, the focus is on investigating the nonreciprocal optical responses of the cold atomic system and its potential use of cavity-free optical isolator and circulator. Considering the D₁ line of cold ⁸⁷Rb atoms, which are cooled to Doppler temperature ($\sim 145\mu\text{K}$), $\gamma_{21} = 10\text{kHz}$ and $\gamma_{31} = \gamma_{41} = \Gamma$ with the spontaneous decay rate of the excited states $2\Gamma = 2\pi \times 5.75\text{MHz}$ [57].

3.1. Optical nonreciprocity via directional FWM effect

The forward-backward transmission characteristics of the probe field passing through the cold atomic medium is explored first. According to Eqs. (7) and (9), the phase diagrams of the forward- and backward-propagating probe fields with the optical depth α ranging from 0 to 600 are plotted in Fig. 2(a). In the phase diagrams, the distance between the data point and origin represents the transmission amplitude ζ_p of the probe field, and the angle between the horizontal axis and a line connecting the origin and data point denotes the corresponding phase shift ϕ_p [61]. As shown in Fig. 2(a), when $\delta_p = \delta_c = 0$ and $\delta_d = 79.6\Gamma$, the forward and backward probe fields have completely different amplitude and phase evolutionary tracks, which means optical nonreciprocity. To obtain deeper insight into the variations of nonreciprocal optical responses, the transmission amplitudes and phase shifts of the forward and backward probe fields versus α are plotted in Figs. 2(b) and 2(c), respectively. It is found that the forward probe field including the amplitude and phase shift oscillates with the increase of the optical depth α , while the

backward probe field exhibits a constantly increasing negative phase shift with the transmission amplitude being slowly decreased [see Figs. 2(b) and 2(c)]. Specifically, when $\alpha = 250$, as indicated by the diamonds in Fig. 2(a), the nonreciprocal transmission arrives at its optimum value with $\zeta_p^f = 0.0379$ and $\zeta_p^b = 0.9609$. When $\alpha = 500$, as indicated by the squares in Fig. 2(a), $\phi_p^f = 0$, $\phi_p^b = -\pi$, $\zeta_p^f = 0.9266$ and $\zeta_p^b = 0.9233$, which means that the optimal nonreciprocal phase shift ($\Delta\phi_p = \phi_p^f - \phi_p^b = \pi$) with high transmission is achieved. In fact, it is feasible to push the optical depth of a cold atomic ensemble up to the 1000 level in experiment [62]. Therefore, the nonreciprocal optical responses can be manipulated by changing the optical depth of the probe transition.

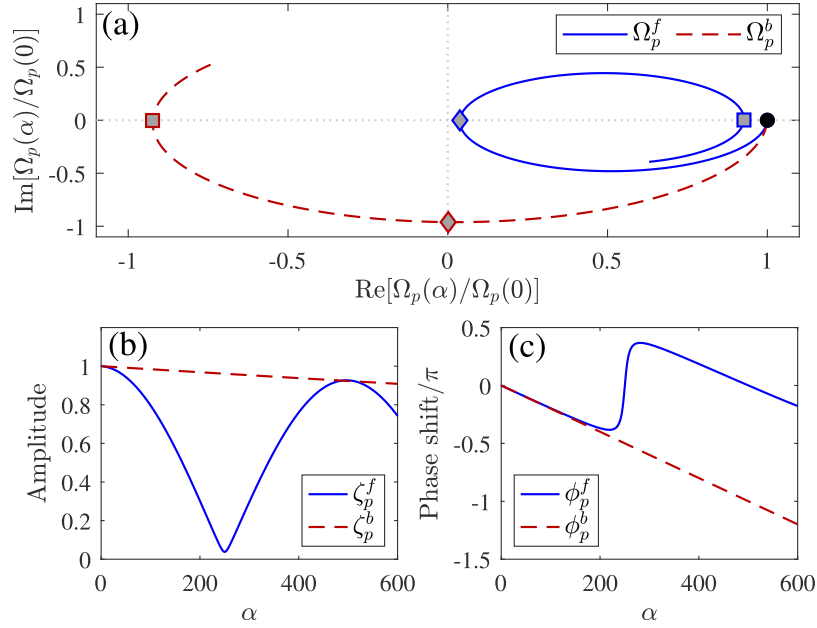


Fig. 2. (a) Phase diagrams of forward and backward probe fields Ω_p^f and Ω_p^b with the optical depth α ranging from 0 to 600. (b) Transmission amplitudes and (c) phase shifts of forward and backward probe fields as a function of α . Other parameters are $\Omega_c = \Omega_d = 12\Gamma$, $\delta_p = \delta_c = 0$ and $\delta_d = 79.6\Gamma$.

The emergence of the optical nonreciprocity, as shown in Fig. 2, originates from the directional phase matching [27]. To better digest the physical mechanism, γ_{21} is set to 0 because of $\gamma_{21} \ll \gamma_{31}, \gamma_{41}, \Omega_c, \Omega_d$ and the focus is directed to the case of $\delta_p = \delta_c = 0$. In this situation, Eqs. (7–9) can be simplified to the following expressions,

$$\Omega_p^f(\alpha) = \Omega_p^f(0) \left[\frac{\Omega_c^2}{\Omega_c^2 + \Omega_d^2} + \frac{\Omega_d^2}{\Omega_c^2 + \Omega_d^2} e^{-\beta\alpha - i\kappa\alpha} \right], \quad (11)$$

$$\Omega_m^f(\alpha) = \Omega_p^f(0) \left[\frac{\Omega_c^* \Omega_d}{\Omega_c^2 + \Omega_d^2} - \frac{\Omega_c^* \Omega_d}{\Omega_c^2 + \Omega_d^2} e^{-\beta\alpha - i\kappa\alpha} \right], \quad (12)$$

$$\Omega_p^b(\alpha) = \Omega_p^b(0) e^{-\frac{1}{2}(\beta\alpha + i\kappa\alpha)}, \quad (13)$$

where $\beta = (\Omega_c^2 + \Omega_d^2)^2 \Gamma^2 / [2\Omega_c^4 \delta_d^2 + 2(\Omega_c^2 + \Omega_d^2)^2 \Gamma^2]$ and $\kappa = \Omega_c^2 (\Omega_c^2 + \Omega_d^2) \delta_d \Gamma / [2\Omega_c^4 \delta_d^2 + 2(\Omega_c^2 + \Omega_d^2)^2 \Gamma^2]$. In the forward case, the phase matching makes the double- Λ system in

Fig. 1(b) form an EIT-based FWM scheme and induces two competing FWM channels, i.e., $|1\rangle \rightarrow |3\rangle \rightarrow |2\rangle \rightarrow |4\rangle \rightarrow |1\rangle$ and $|1\rangle \rightarrow |4\rangle \rightarrow |2\rangle \rightarrow |3\rangle \rightarrow |1\rangle$. The large driving detuning δ_d causes an imbalance between the two FWM channels and leads to the power oscillation between the probe and FWM fields. When $\alpha = 250$ (500), $\kappa\alpha = \pi$ (2π), and almost all of the photon energy is converted from the probe (FWM) field to the FWM (probe) field with zero phase shift [see Eqs. (11) and (12)]. However, in the backward case, a N -type EIT system is formed owing to the lack of phase matching [see Fig. 1(c)]. It is clear from Eq. (13) that the large driving detuning δ_d reduces the absorption coefficient $\beta/2$, thereby leading to most probe photons being routed in the backward direction.

According to Eqs. (11) and (13), it can be found that the driving detuning δ_d greatly influences the absorption term $\beta\alpha$ and the phase term $\kappa\alpha$, which determines the nonreciprocal optical responses of the cold atomic system. Figures 3(a) and 3(b) display the variations of the transmission amplitudes and phase shifts of the forward and backward probe fields with the driving detuning δ_d , respectively. This clearly shows that the nonreciprocal phase shift reaches the optimal effect (i.e., $\Delta\phi_p = \pi$) with high transmission at $\delta_d = 79.6\Gamma$, while the nonreciprocal transmission arrives at the optimal effect at $\delta_d = 159.2\Gamma$. Therefore, the detuning of the driving field can manipulate the nonreciprocal behaviors of the forward and backward probe fields by an optical method. This indicates that magnetic-free optical nonreciprocity with all-optical controllable capability can be achieved with enhanced FWM effect in a cold atomic medium.

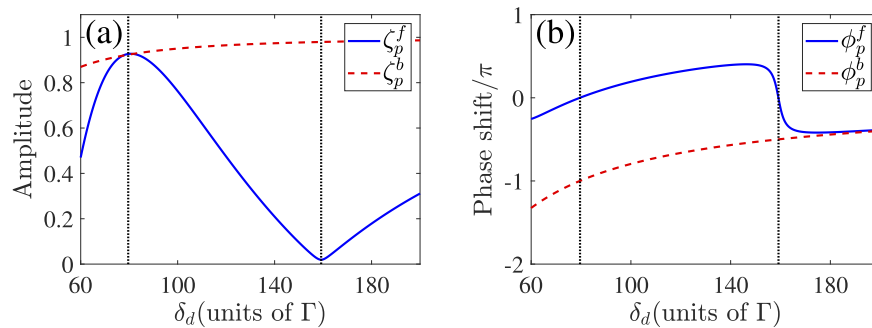


Fig. 3. (a) Transmission amplitudes and (b) phase shifts of forward and backward probe fields as a function of the driving detuning δ_d . Other parameters are the same as in Fig. 2(b), except for $\alpha = 500$.

3.2. Application: optical isolator and circulator

It has been demonstrated that the controllable optical nonreciprocity is well suitable for application in nonreciprocal photonic devices, such as optical isolators [13,18,27,29], circulators [15,17] and directional amplifiers [17,45]. Previous study [63] has shown that a nonreciprocal phase shifter embedded in a Mach-Zehnder interferometer (MZI) provides a practical and effective platform for designing cavity-free optical isolators and circulators. In our work, the MZI is built by using two polarization-maintained fiber beam splitters (BSs). The two BSs are used to first divide the input probe field into two branches and then mix them. A vapor cell filled with cold ^{87}Rb atoms acts as a nonreciprocal phase shifter and is then connected to the upper branch of the MZI [see Fig. 4]. Cold atomic medium with ultrahigh optical depth can be achieved by a convenient magneto-optical trap setup [62]. Besides, the effect of the magnetic fields on nonreciprocal phase shift can be neglected because the frequency shift of Zeeman states can be reduced to a few kHz or less via using three pairs of magnetic coils to compensate the background magnetic field [55]. As shown in Fig. 4, a pinhole (P), a polarization beam splitter (PBS), two half-wave plates (HWPs), two quarter-wave plates (QWPs) and two lenses (Ls) are located at the upper

branch of the MZI. The scattering of the coupling and driving beams can be blocked by P. Ls can realize the coupling of spatial light to optical fiber. HWPs and QWPs can convert the polarization states of the applied fields between vertical (horizontal) polarization and left (right) circular polarization to guarantee the effective light-atom interaction. The incident forward and backward probe fields are vertically polarized and can transmit through PBS, while the generated forward FWM field can be converted from right circular polarization to horizontal polarization, which can be decoupled from the upper branch of the MZI via the reflection of PBS. Because of the nonreciprocal phase shift induced by the directional FWM effect, the probe photons accumulate different phase shifts when propagating along the upper and lower branches of the MZI, and then interfere constructively or destructively at the end of the interferometer. Here, two BSs are chosen to be identical and then the input-output relation of the two beam splitters can be written as [64]

$$\hat{a}_{out}^\dagger = \cos \theta \hat{a}_{in}^\dagger + ie^{-i\varphi} \sin \theta \hat{b}_{in}^\dagger, \quad (14)$$

$$\hat{b}_{out}^\dagger = ie^{i\varphi} \sin \theta \hat{a}_{in}^\dagger + \cos \theta \hat{b}_{in}^\dagger, \quad (15)$$

in which $\sin \theta$ and $\cos \theta$ are the reflection and transmission amplitudes of the beam splitter, respectively. φ represents the relative phase between the reflection and transmission amplitudes. Combining Eqs. (10), (14) and (15), the transmission matrix elements between the input and output ports are obtained as

$$T_{12} = \left| \frac{a_{2,out}}{a_{1,in}} \right|^2 = \left| \zeta_p^f e^{i\phi_p^f} \cos^2 \theta - \sin^2 \theta \right|^2, \quad (16)$$

$$T_{21} = \left| \frac{a_{1,out}}{a_{2,in}} \right|^2 = \left| \zeta_p^b e^{i\phi_p^b} \cos^2 \theta - \sin^2 \theta \right|^2, \quad (17)$$

$$T_{14} = \left| \frac{b_{2,out}}{a_{1,in}} \right|^2 = \left| (1 + \zeta_p^f e^{i\phi_p^f}) \cos \theta \sin \theta \right|^2, \quad (18)$$

$$T_{41} = \left| \frac{a_{1,out}}{b_{2,in}} \right|^2 = \left| (1 + \zeta_p^b e^{i\phi_p^b}) \cos \theta \sin \theta \right|^2, \quad (19)$$

$$T_{32} = \left| \frac{a_{2,out}}{b_{1,in}} \right|^2 = \left| (1 + \zeta_p^f e^{i\phi_p^f}) \cos \theta \sin \theta \right|^2, \quad (20)$$

$$T_{23} = \left| \frac{b_{1,out}}{a_{2,in}} \right|^2 = \left| (1 + \zeta_p^b e^{i\phi_p^b}) \cos \theta \sin \theta \right|^2, \quad (21)$$

$$T_{34} = \left| \frac{b_{2,out}}{b_{1,in}} \right|^2 = \left| \cos^2 \theta - \zeta_p^f e^{i\phi_p^f} \sin^2 \theta \right|^2, \quad (22)$$

$$T_{43} = \left| \frac{b_{1,out}}{b_{2,in}} \right|^2 = \left| \cos^2 \theta - \zeta_p^b e^{i\phi_p^b} \sin^2 \theta \right|^2, \quad (23)$$

where T_{mn} is the transmission coefficient from port m to port n , with $m, n = 1, 2, 3, 4$. It is assumed that the backscattering caused by the fiber roughness is negligible, so T_{mm} ($m = 1, 2, 3, 4$) is set to zero. For the same reason, the photons injected from port 1 can not pass through port 3, which implies that $T_{13} = 0$. With similar arguments, we have $T_{24} = T_{31} = T_{42} = 0$. In addition, the relevant parameters $\alpha = 500$, $\Omega_c = \Omega_d = 12\Gamma$, $\delta_c = 0$ and $\delta_d = 79.6\Gamma$ are also chosen for the cold atomic ensemble.

First, a cavity-free optical isolator is implemented by selecting port 1 and port 2 of the MZI. Based on Eqs. (16) and (17), the reflection of the beam splitter is precisely set to

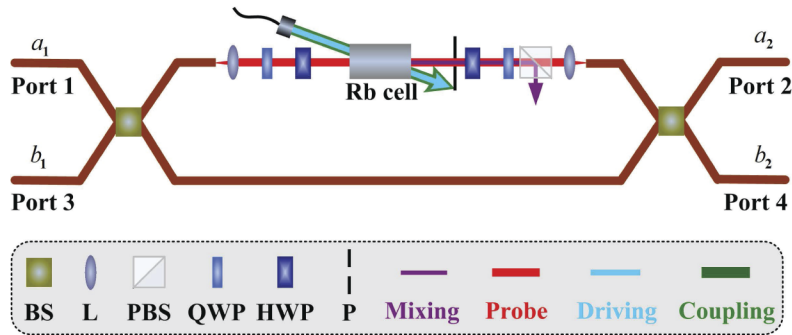


Fig. 4. Schematic for proposed optical isolator and circulator based on a Mach-Zehnder interferometer, in which atomic cell filled by cold ^{87}Rb atoms is accessed to upper branch. **BS:** beam splitter, **L:** lens, **PBS:** polarization beam splitter, **QWP:** quarter-wave plate, **HWP:** half-wave plate; **P:** pinhole.

$\sin^2 \theta = \zeta_p^{f,opt} / (1 + \zeta_p^{f,opt}) \approx 0.4810$. In this situation, the forward transmission T_{12} and the backward transmission T_{21} of the probe field versus the probe detuning δ_p are plotted separately in Fig. 5(a). It is found that the forward and backward transmission coefficients are very different. Specifically, the forward transmission T_{12} first decreases and then increases at a low level with δ_p increasing from -0.4Γ to 0.4Γ [see blue solid line in Fig. 5(a)], while the backward transmission T_{21} exhibits the opposite trend at a high level [see red dashed line in Fig. 5(a)]. In this region, the backward transmission T_{21} far outweighs T_{12} , which implies that the probe photons are transmitted in the backward direction and blocked in the forward direction. Therefore, the backward propagating probe field is actually the transmitted signal for two-port cavity-free optical isolator.

The performance of an optical isolator can be quantified by the isolation ratio IR and insertion loss IL [18,47], which are defined as $IR = 10 \log_{10} |a_{1,out}/a_{2,out}|^2 = -10 \log_{10}(T_{12}/T_{21})$ and $IL = 10 \log_{10} |a_{2,in}/a_{1,out}|^2 = -10 \log_{10} T_{21}$, respectively. In Figs. 5(b) and 5(c), the isolation ratio IR and insertion loss IL of the optical isolator are plotted versus the probe detuning δ_p . It is found that the isolation ratio reaches the maximum of 79.70 dB at the optimal point $\delta_p^{opt} = 0$ and decreases rapidly with the variation of δ_p [see blue solid line in Fig. 5(b)]. At the same time, the insertion loss is only 0.35 dB for the optimal isolation ratio [see Fig. 5(c)]. In comparison with previous schemes [47,48], the proposed cavity-free optical isolator is a great improvement. In the case of low insertion loss (i.e., $IL < 1$ dB), it is roughly twice the maxima isolation ratio (i.e., $IR \sim 40$ dB) in Ref. [47] and four times the maxima isolation ratio (i.e., $IR \sim 20$ dB) in Ref. [48]. Besides, the isolation ratio can reach more than 20 dB in the range of $-0.209\Gamma \leq \delta_p \leq 0.207\Gamma$, yielding an isolation bandwidth of $\pi \times 2.39\text{MHz}$ [see blue solid line in Fig. 5(b)], in which the insertion loss is less than 0.66 dB [see Fig. 5(c)]. This shows that cavity-free optical isolator can be realized with enhanced FWM effect in a cold atomic medium. Furthermore, in the case of imperfect input coupling, the disturbance of the input intensities of the coupling and driving fields is considered. By introducing random variations into the intensities of the coupling and driving fields, the corresponding Rabi frequencies can be rewritten as $\Omega_c = \Omega_{c0} + \delta\Omega_c \cdot \{\zeta_j\}$ and $\Omega_d = \Omega_{d0} + \delta\Omega_d \cdot \{\tau_j\}$, where Ω_{c0} and Ω_{d0} are the intensities of the coupling and driving fields in the perfect input coupling case. $\delta\Omega_c$ and $\delta\Omega_d$ are the ranges of disturbance in the intensities of the coupling and driving fields. $\{\zeta_j\}$ and $\{\tau_j\}$ represent sequences of uncorrelated random numbers with standard normal distribution. Here, $\Omega_{c0} = \Omega_{d0} = 12\Gamma$ and $\delta\Omega_c = \delta\Omega_d = 0.002\Omega_{c0} = 0.024\Gamma$ are considered. It can be seen that the random disturbance in the intensities of the coupling and driving fields results in the perturbation of isolation ratio [see red dots in Fig. 5(b)]. Actually, the output amplitudes and phase shifts of the forward and backward probe fields described by Eqs. (7)

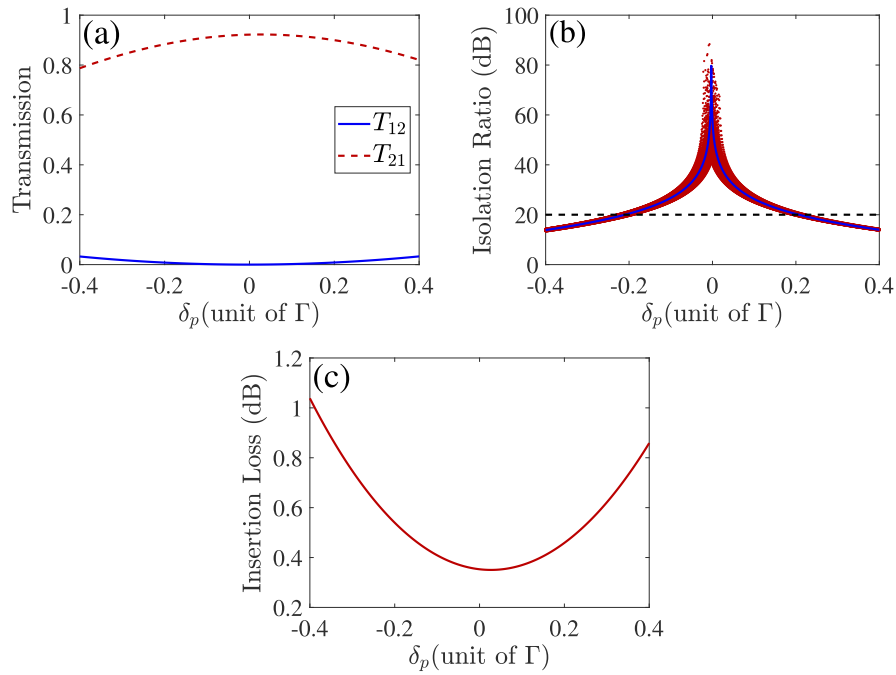


Fig. 5. (a) Transmission coefficients T_{12} and T_{21} , (b) isolation ratio IR and (c) insertion loss IL of an optical isolator as a function of the probe detuning δ_p . The blue solid line in Fig. 5(b) represents the perfect input coupling case, while red dots represent the set of 50 random disturbances of the isolation ratio in the imperfect input coupling case. Other parameters are the same as in Fig. 2 except for $\alpha = 500$.

and (9) depend on the intensities of the coupling and driving fields. The random disturbance in Ω_c and Ω_d would cause the fluctuation of the transmission coefficients between port 1 and port 2, which results in the find in Fig. 5(b). More importantly, one can find that the overall isolation performance, including effective isolation ratio and bandwidth, becomes worse in comparison with the case of perfect input coupling.

Second, a cavity-free optical circulator is implemented with the four ports of the MZI. According to Eqs. (16–23), the beam splitter with the reflection $\sin^2 \theta = 1/2$ is chosen so as to balance the probe photons propagating in the MZI. To explore the circulation function of the four-port optical circulator shown in Fig. 4, the transmission coefficients are plotted versus the probe detuning δ_p in the forward-circulation direction ($1 \rightarrow 2 \rightarrow 3 \rightarrow 4 \rightarrow 1$) and the backward-circulation direction ($1 \rightarrow 4 \rightarrow 3 \rightarrow 2 \rightarrow 1$) in Figs. 6(a) and 6(b), respectively. It is found that the probe photons present nonreciprocal transmission in the forward- and backward-circulation directions. The forward-circulation transmission $T_{i,i+1}$ ($i = 1, 2, 3, 4$) first decreases and then increases, while the transmission $T_{i+1,i}$ in the backward-circulation direction shows the opposite trend with increasing δ_p , which are similar to the case shown in Fig. 5(a). At the optimal point $\delta_p^{\text{opt}} = 0$, the lowest forward-circulation transmissions (0.14% ~ 0.15%) are achieved with relative high backward-circulation transmissions (92.47% ~ 92.79%), implying that the probe photons circulate along the direction of $1 \rightarrow 4 \rightarrow 3 \rightarrow 2 \rightarrow 1$.

For an optical circulator, the fidelity F and average photon survival probability η are adopted in appraising the performance of the circulation function [1,47]. The operational fidelity of the optical circulator is calculated by $F = \text{Tr}[\tilde{T}T^{\text{id},T}]/\text{Tr}[T^{\text{id}}T^{\text{id},T}]$, with $T^{\text{id}} =$

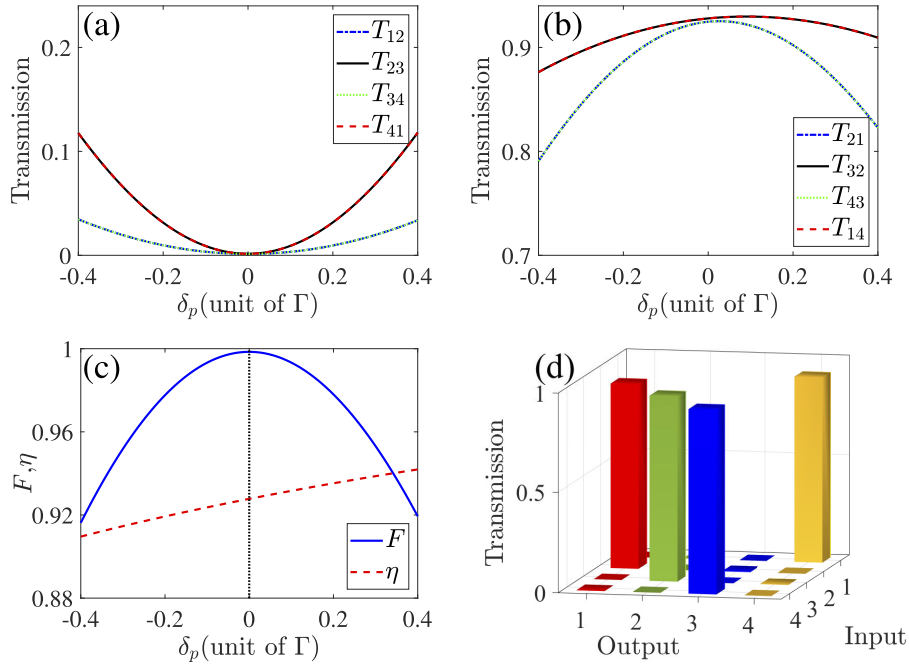


Fig. 6. (a) Forward-circulation and (b) backward-circulation transmission coefficients as a function of the probe detuning δ_p . (c) Fidelity F and average survival probability η of an optical circulator as a function of the probe detuning δ_p . (d) Transmission matrices for an optical circulator at the optimal point $\delta_p^{\text{opt}} = 0$. Other parameters are the same as in Fig. 2 except for $\alpha = 500$.

$[0, 0, 0, 1; 1, 0, 0, 0; 0, 1, 0, 0; 0, 0, 1, 0]$ and $\tilde{T} = (T_{ij}/\eta_i)$ being the ideal and renormalized transmission matrices, respectively. $\eta_i = \sum_k T_{i,k}$ is the survival probability of probe photons entering port i . Note that the range of fidelity F is from 0 to 1, in which $F = 1$ corresponds to an ideal operation circulator. The average photon survival probability is calculated by $\eta = \sum_i \eta_i/4$. In Fig. 6(c), F and η are presented separately as a function of the probe detuning δ_p . One can find that the maximal fidelity of 0.9985 occurs at $\delta_p^{\text{opt}} = 0$, where the average photon survival probability has a high value of 0.9278. Figure 6(d) shows the complete 4×4 transmission matrix of the optical circulator with the optimal fidelity, which is very close to the ideal transmission matrix T^{id} . Besides displaying a good optical nonreciprocity, the transmission matrix is also used to calculate the per-channel isolation ratio and insertion loss via $IR_i = -10 \log_{10}(T_{i,i+1}/T_{i+1,i})$ and $IL_i = -10 \log_{10} T_{i+1,i}$, respectively. At $\delta_p^{\text{opt}} = 0$, we can obtain $\{IR_i\} = \{28.36, 27.99, 28.36, 27.99\}$ dB and $\{IL_i\} = \{0.34, 0.32, 0.34, 0.32\}$ dB with $i = \{1, 2, 3, 4\}$. It can be seen that the four channels have almost the same isolation ratio and insertion loss. The average insertion loss IL is only 0.33 dB. Table 1 lists the performance metrics of three optical circulators including fidelity F , average photon survival probability η and average insertion loss IL . From Table 1, it can be seen that the proposed optical circulator has higher fidelity and average photon survival probability and lower average insertion loss compared with previous schemes [47,49], which shows better performance of circulation. This indicates that cavity-free optical circulator can also be realized with enhanced FWM effect in a cold atomic medium.

Before concluding, it should be noted that our nonreciprocal system can operate at low light level. Previous study has demonstrated that nonlinear optical processes at low light level can

Table 1. Comparing of the performance metrics for three optical circulators

Optical circulator	Fidelity F	Average photon survival probability η	Average insertion loss IL (dB)
Ref. [47]	0.94	0.72	1.42
Ref. [49]	0.98	0.85	0.7
Our proposal	0.9985	0.9278	0.33

be achieved in an atomic ensemble via the combination of EIT and cold atom technology [52]. In particular, a low-light-level FWM has been experimentally observed in cold ^{87}Rb atomic ensemble via using a driving pulse with a peak intensity of $\approx 80\mu\text{W}/\text{cm}^2$, corresponding to an energy of ≈ 60 photons per atomic cross section [55]. In the weak probe field approximation, the intensity of the probe field is far smaller than the intensities of the control and driving fields. Therefore, the probe field may have an energy of a few photons per atomic cross section, corresponding to low light level. In this case, the intensity of the probe field is so weaker that it has little influence on nonreciprocal transmission and nonreciprocal phase shift. Our proposal is experimentally realizable because optical nonreciprocity [44,49] and enhanced FWM process [54,55] have been experimentally implemented in the atomic ensemble.

4. Conclusions

In conclusion, a scheme for realizing and manipulating the optical nonreciprocity in an ensemble of cold ^{87}Rb atoms is theoretically suggested. Owing to the dependence of the FWM effect on the directional phase matching, the forward and backward probe fields suffer different evolutions for the probe transmission and phase shift. It is demonstrated that the nonreciprocal transmission and nonreciprocal phase shift can be effectively manipulated via adjusting the optical depth and driving detuning. Moreover, based on the achievable nonreciprocal phase shift with high transmission, a two-port optical isolator and a four-port optical circulator are designed by inserting cold atoms into a MZI. By properly choosing the parameters of the system, the optimal isolation ratio and insertion loss of the optical isolator can reach 79.90 dB and 0.35 dB, respectively, and the optical circulator has a fidelity of 0.9985 and a photon survival probability of 0.9278. These performance metrics are greatly improved compared with previous schemes [47–49]. An EIT-based FWM has been experimentally observed at low light level [55]. Thus, the proposed scheme paves a path toward optically controllable cavity-free nonreciprocal photonic devices at low light level and may have potential applications in quantum network and quantum information process.

Up to now, the proposed question in Sec. 1. is well solved. The study states clearly that magnetic-free optical nonreciprocity can be achieved and cavity-free nonreciprocal photonic devices can be realized with enhanced FWM effect in a cold atomic medium.

Appendix: Equations of motion for the density matrices in the forward and backward propagation cases

In this appendix, we describe the equations of motion of the density matrices and derive the corresponding off-diagonal matrix elements for the forward and backward propagation cases shown in Fig. 1.

For the forward propagation case, the weak probe field propagates through the cold atomic medium in the forward (+z) direction. In this situation, the probe, coupling and driving fields (Ω_p^f , Ω_c , Ω_d) interact with the four-level ^{87}Rb atoms and generate a forward FWM field Ω_m^f via FWM effect owing to the presence of phase matching. Under the electric-dipole and rotating-wave approximations, as shown in Fig. 1(b), the interaction Hamiltonian in the interaction picture for

the double- Λ -type atomic system is given by

$$H_I^f = -\hbar[\Delta_1|3\rangle\langle 3| + \Delta_2|2\rangle\langle 2| + \Delta_3|4\rangle\langle 4| + (\Omega_c|3\rangle\langle 2| + \Omega_d|4\rangle\langle 2| + \Omega_p^f|3\rangle\langle 1| + \Omega_m^f|4\rangle\langle 1| + H.c.)], \quad (24)$$

where $H.c.$ means Hermitian conjugate. $\Delta_1 = \delta_p$, $\Delta_2 = \delta_p - \delta_c$ and $\Delta_3 = \delta_p - \delta_c + \delta_d$ represent the one-photon, two-photon and three-photon detunings, respectively. $\delta_p = \omega_p - \omega_{31}$, $\delta_c = \omega_c - \omega_{32}$ and $\delta_d = \omega_d - \omega_{42}$ are the detunings of the probe, coupling and driving fields, respectively. The equations of motion for the density matrix elements can be obtained as

$$\frac{\partial \rho_{21}^f}{\partial t} = i(\Delta_2 + i\gamma_{21})\rho_{21}^f + i\Omega_c^*\rho_{31}^f + i\Omega_d^*\rho_{41}^f + i\Omega_p^f\rho_{23}^f - i\Omega_m^f\rho_{24}^f, \quad (25)$$

$$\frac{\partial \rho_{31}^f}{\partial t} = i(\Delta_1 + i\gamma_{31})\rho_{31}^f + i\Omega_p^f(\rho_{11}^f - \rho_{33}^f) + i\Omega_c\rho_{21}^f - i\Omega_m^f\rho_{34}^f, \quad (26)$$

$$\frac{\partial \rho_{41}^f}{\partial t} = i(\Delta_3 + i\gamma_{41})\rho_{41}^f + i\Omega_m^f(\rho_{11}^f - \rho_{44}^f) + i\Omega_d\rho_{21}^f - i\Omega_p^f\rho_{43}^f. \quad (27)$$

It is assumed that the probe and FWM fields are much smaller than the coupling and driving fields so that almost all atoms will remain in the level $|1\rangle$, i.e. $\rho_{11}^f = 1$ and $\rho_{22}^f = \rho_{33}^f = \rho_{44}^f = 0$. According to Eqs. (25–27), the steady-state solutions of the corresponding off-diagonal matrix elements ρ_{31}^f and ρ_{41}^f can be obtained straightforwardly as

$$\rho_{31}^f = \frac{-(\Omega_d^2 - d_{21}d_{41})\Omega_p^f + \Omega_c\Omega_d^*\Omega_m^f}{\Omega_d^2d_{31} + \Omega_c^2d_{41} - d_{21}d_{31}d_{41}}, \quad (28)$$

$$\rho_{41}^f = \frac{-(\Omega_c^2 - d_{21}d_{31})\Omega_m^f + \Omega_c^*\Omega_d\Omega_p^f}{\Omega_d^2d_{31} + \Omega_c^2d_{41} - d_{21}d_{31}d_{41}}, \quad (29)$$

where $d_{21} = \Delta_2 + i\gamma_{21}$, $d_{31} = \Delta_1 + i\gamma_{31}$ and $d_{41} = \Delta_3 + i\gamma_{41}$. $2\gamma_{j1}$ ($j = 2, 3, 4$) is the decay rate of the coherence between the states $|j\rangle$ and $|1\rangle$.

In the backward propagation case, the weak probe field propagates along with the direction of $-z$ axis. Due to the lack of phase matching, no FWM field is generated when the backward probe field passes through the cold atomic medium. Thus, as shown in Fig. 1(c), the interaction Hamiltonian for the N -type atomic system can be written as

$$H_I^b = -\hbar[\Delta_1|3\rangle\langle 3| + \Delta_2|2\rangle\langle 2| + \Delta_3|4\rangle\langle 4| + (\Omega_c|3\rangle\langle 2| + \Omega_d|4\rangle\langle 2| + \Omega_p^b|3\rangle\langle 1| + H.c.)]. \quad (30)$$

And then the equations of motion for the density matrix elements are given by

$$\frac{\partial \rho_{21}^b}{\partial t} = i(\Delta_2 + i\gamma_{21})\rho_{21}^b + i\Omega_c^*\rho_{31}^b + i\Omega_d^*\rho_{41}^b + i\Omega_p^b\rho_{23}^b, \quad (31)$$

$$\frac{\partial \rho_{31}^b}{\partial t} = i(\Delta_1 + i\gamma_{31})\rho_{31}^b + i\Omega_p^b(\rho_{11}^b - \rho_{33}^b) + i\Omega_c\rho_{21}^b, \quad (32)$$

$$\frac{\partial \rho_{41}^b}{\partial t} = i(\Delta_3 + i\gamma_{41})\rho_{41}^b + i\Omega_d\rho_{21}^b - i\Omega_p^b\rho_{43}^b. \quad (33)$$

In the limit of the weak backward probe field, almost all atoms will remain in the level $|1\rangle$, i.e. $\rho_{11}^b = 1$ and $\rho_{22}^b = \rho_{33}^b = \rho_{44}^b = 0$. According to Eqs. (31–33), the steady-state solution of the

corresponding off-diagonal matrix element ρ_{31}^b can be derived as

$$\rho_{31}^b = -\frac{(\Omega_d^2 - d_{21}d_{41})\Omega_p^b}{\Omega_d^2 d_{31} + \Omega_c^2 d_{41} - d_{21}d_{31}d_{41}}. \quad (34)$$

It is assumed that $D_p = \Omega_d^2 - d_{21}d_{41}$, $D_m = \Omega_c^2 - d_{21}d_{31}$ and $D = \Omega_d^2 d_{31} + \Omega_c^2 d_{41} - d_{21}d_{31}d_{41}$. Then, the off-diagonal matrix elements shown in Eqs. (1–3) of the main text are achieved.

Funding. National Natural Science Foundation of China (11774054, 12075036, 12104067); Science and Technology Research Project of Education Department of Hubei Province (Q20211314).

Disclosures. The authors declare no conflicts of interest.

Data availability. Data underlying the results presented in this paper are not publicly available at this time but may be obtained from the authors upon reasonable request.

References

1. M. Scheucher, A. Hilico, E. Will, J. Volz, and A. Rauschenbeutel, "Quantum optical circulator controlled by a single chirally coupled atom," *Science* **354**(6319), 1577–1580 (2016).
2. D. Jalas, A. Y. Petrov, M. Eich, W. Freude, S. Fan, Z. Yu, R. Baets, M. A. Popovic, A. Melloni, J. D. Joannopoulos, M. Vanwolleghem, C. R. Doerr, and H. Renner, "What is - and what is not - an optical isolator," *Nat. Photonics* **7**(8), 579–582 (2013).
3. F. D. M. Haldane and S. Raghu, "Possible realization of directional optical waveguides in photonic crystals with broken time-reversal symmetry," *Phys. Rev. Lett.* **100**(1), 013904 (2008).
4. L. Bi, J. Hu, P. Jiang, D. H. Kim, G. F. Dionne, L. C. Kimerling, and C. A. Ross, "On-chip optical isolation in monolithically integrated non-reciprocal optical resonators," *Nat. Photonics* **5**(12), 758–762 (2011).
5. Z. Yu and S. Fan, "Complete optical isolation created by indirect interband photonic transitions," *Nat. Photonics* **3**(2), 91–94 (2009).
6. Z. Yu and S. Fan, "Optical isolation based on nonreciprocal phase shift induced by interband photonic transitions," *Appl. Phys. Lett.* **94**(17), 171116 (2009).
7. D. Po, "Travelling-wave Mach-Zehnder modulators functioning as optical isolators," *Opt. Express* **23**(8), 10498–10505 (2015).
8. K. Fang, Z. Yu, and S. Fan, "Photonic aharonov-bohm effect based on dynamic modulation," *Phys. Rev. Lett.* **108**(15), 153901 (2012).
9. B. Abdo, K. Sliwa, L. Frunzio, and M. Devoret, "Directional amplification with a josephson circuit," *Phys. Rev. X* **3**(3), 031001 (2013).
10. D. L. Sounas, C. Caloz, and A. Alù, "Giant non-reciprocity at the subwavelength scale using angular momentum-biased metamaterials," *Nat. Commun.* **4**(1), 2407 (2013).
11. D. L. Sounas and A. Alù, "Angular-momentum-biased nanorings to realize magnetic-free integrated optical isolation," *ACS Photonics* **1**(3), 198–204 (2014).
12. N. A. Estep, D. L. Sounas, J. Soric, and A. Alù, "Magnetic-free non-reciprocity and isolation based on parametrically modulated coupled-resonator loops," *Nat. Phys.* **10**(12), 923–927 (2014).
13. M. S. Kang, A. Butsch, and P. S. J. Russell, "Reconfigurable light-driven opto-acoustic isolators in photonic crystal fibre," *Nat. Photonics* **5**(9), 549–553 (2011).
14. S. Manipatruni, J. T. Robinson, and M. Lipson, "Optical nonreciprocity in optomechanical structures," *Phys. Rev. Lett.* **102**(21), 213903 (2009).
15. X. W. Xu and Y. Li, "Optical nonreciprocity and optomechanical circulator in three-mode optomechanical systems," *Phys. Rev. A* **91**(5), 053854 (2015).
16. Z. Shen, Y. L. Zhang, Y. Chen, C. L. Zou, Y. F. Xiao, X. B. Zou, F. W. Sun, G. C. Guo, and C. H. Dong, "Experimental realization of optomechanically induced non-reciprocity," *Nat. Photonics* **10**(10), 657–661 (2016).
17. Z. Shen, Y. L. Zhang, Y. Chen, F. W. Sun, X. B. Zou, G. C. Guo, C. L. Zou, and C. H. Dong, "Reconfigurable optomechanical circulator and directional amplifier," *Nat. Commun.* **9**(1), 1797 (2018).
18. F. Ruesink, M.-A. Miri, A. Alu, and E. Verhagen, "Nonreciprocity and magnetic-free isolation based on optomechanical interactions," *Nat. Commun.* **7**(1), 13662 (2016).
19. K. Xia, G. Lu, G. Lin, Y. Cheng, and J. Twamley, "Reversible nonmagnetic single-photon isolation using unbalanced quantum coupling," *Phys. Rev. A* **90**(4), 043802 (2014).
20. C. Sayrin, C. Junge, R. Mitsch, B. Albrecht, D. O'Shea, P. Schneeweiss, J. Volz, and A. Rauschenbeutel, "Nanophotonic optical isolator controlled by the internal state of cold atoms," *Phys. Rev. X* **5**(4), 041036 (2015).
21. L. Jin and Z. Song, "Incident direction independent wave propagation and unidirectional lasing," *Phys. Rev. Lett.* **121**(7), 073901 (2018).
22. L. Jin and Z. Song, "Symmetry-protected scattering in non-Hermitian linear systems," *Chin. Phys. Lett.* **38**(2), 024202 (2021).

23. V. Grigoriev and F. Biancalana, "Nonreciprocal switching thresholds in coupled nonlinear microcavities," *Opt. Lett.* **36**(11), 2131–2133 (2011).
24. L. Del Bino, M. J. Silver, M. T. M. Woodley, S. L. Stebbings, X. Zhao, and P. Del'Haye, "Microresonator isolators and circulators based on the intrinsic nonreciprocity of the Kerr effect," *Optica* **5**(3), 279–282 (2018).
25. L. Fan, J. Wang, L. T. Varghese, H. Shen, B. Niu, Y. Xuan, A. M. Weiner, and M. Qi, "An all-silicon passive optical diode," *Science* **335**(6067), 447–450 (2012).
26. J. Kim, M. C. Kuzyk, K. Han, H. Wang, and G. Bahl, "Non-reciprocal Brillouin scattering induced transparency," *Nat. Phys.* **11**(3), 275–280 (2015).
27. S. Hua, J. Wen, X. Jiang, Q. Hua, L. Jiang, and M. Xiao, "Demonstration of a chip-based optical isolator with parametric amplification," *Nat. Commun.* **7**(1), 13657 (2016).
28. K. Wang, S. Gao, Y. Wang, A. Nirmalathas, C. Lim, K. Alameh, and E. Skafidas, "Four-wave-mixing-based silicon integrated optical isolator with dynamic non-reciprocity," *IEEE Photonics Technol. Lett.* **28**(16), 1739–1742 (2016).
29. L. Chang, X. Jiang, S. Hua, C. Yang, J. Wen, L. Jiang, G. Li, G. Wang, and M. Xiao, "Parity–time symmetry and variable optical isolation in active–passive-coupled microresonators," *Nat. Photonics* **8**(7), 524–529 (2014).
30. B. Peng, S. K. Özdemir, F. Lei, F. Monifi, M. Gianfreda, G. L. Long, S. Fan, F. Nori, C. M. Bender, and L. Yang, "Parity–time-symmetric whispering-gallery microcavities," *Nat. Phys.* **10**(5), 394–398 (2014).
31. S. E. Harris, "Electromagnetically induced transparency," *Phys. Today* **50**(7), 36–42 (1997).
32. Y. Wu and X. Yang, "Electromagnetically induced transparency in V-, Λ -, and cascade-type schemes beyond steady-state analysis," *Phys. Rev. A* **71**(5), 053806 (2005).
33. M. D. Lukin and A. Imamoglu, "Controlling photons using electromagnetically induced transparency," *Nature* **413**(6853), 273–276 (2001).
34. S. A. Carvalho and L. E. E. de Araujo, "Electromagnetically induced blazed grating at low light levels," *Phys. Rev. A* **83**(5), 053825 (2011).
35. T. Shui, W.-X. Yang, L. Li, and X. Wang, "Lop-sided Raman-Nath diffraction in PT-antisymmetric atomic lattices," *Opt. Lett.* **44**(8), 2089–2092 (2019).
36. L. V. Hau, S. E. Harris, Z. Dutton, and C. H. Behroozi, "Light speed reduction to 17 metres per second in an ultracold atomic gas," *Nature* **397**(6720), 594–598 (1999).
37. D. Han, H. Guo, Y. Bai, and H. Sun, "Subluminal and superluminal propagation of light in an N-type medium," *Phys. Lett. A* **334**(2-3), 243–248 (2005).
38. C. Hang, G. Huang, and V. V. Konotop, "PT-symmetry with a system of three-level atoms," *Phys. Rev. Lett.* **110**(8), 083604 (2013).
39. J. H. Wu, M. Artoni, and G. C. La Rocca, "Non-Hermitian degeneracies and unidirectional reflectionless atomic lattices," *Phys. Rev. Lett.* **113**(12), 123004 (2014).
40. D. Wang, H. Zhou, M. Guo, J. Zhang, J. Evers, and S. Zhu, "Optical diode made from a moving photonic crystal," *Phys. Rev. Lett.* **110**(9), 093901 (2013).
41. S. A. R. Horsley, J.-H. Wu, M. Artoni, and G. C. La Rocca, "Optical nonreciprocity of cold atom Bragg mirrors in motion," *Phys. Rev. Lett.* **110**(22), 223602 (2013).
42. L. Yang, Y. Zhang, X.-B. Yan, Y. Sheng, C.-L. Cui, and J.-H. Wu, "Dynamically induced two-color nonreciprocity in a tripod system of a moving atomic lattice," *Phys. Rev. A* **92**(5), 053859 (2015).
43. H. Ramezani, P. K. Jha, Y. Wang, and X. Zhang, "Nonreciprocal localization of photons," *Phys. Rev. Lett.* **120**(4), 043901 (2018).
44. S. Zhang, Y. Hu, G. Lin, Y. Niu, K. Xia, J. Gong, and S. Gong, "Thermal-motion-induced non-reciprocal quantum optical system," *Nat. Photonics* **12**(12), 744–748 (2018).
45. G. Lin, S. Mang, Y. Hu, Y. Niu, J. Gong, and S. Gong, "Nonreciprocal amplification with four-level hot atoms," *Phys. Rev. Lett.* **123**(3), 033902 (2019).
46. C. Liang, B. Liu, A.-N. Xu, X. Wen, C. Lu, K. Xia, M. K. Tey, Y.-C. Liu, and L. You, "Collision-induced broadband optical nonreciprocity," *Phys. Rev. Lett.* **125**(12), 123901 (2020).
47. K. Xia, F. Nori, and M. Xiao, "Cavity-free optical isolators and circulators using a chiral cross-Kerr nonlinearity," *Phys. Rev. Lett.* **121**(20), 203602 (2018).
48. E. Z. Li, D. S. Ding, Y. C. Yu, M. X. Dong, L. Zeng, W. H. Zhang, Y. H. Ye, H. Z. Wu, Z. H. Zhu, W. Gao, G. C. Guo, and B. S. Shi, "Experimental demonstration of cavity-free optical isolators and optical circulators," *Phys. Rev. Res.* **2**(3), 033517 (2020).
49. S. Zhang, G. Lin, Y. Hu, Y. Qi, and S. Gong, "Cavity-free circulator with low insertion loss using hot atoms," *Phys. Rev. Appl.* **14**(2), 024032 (2020).
50. S. E. Harris and A. Imamoglu, "Nonlinear optical processes using electromagnetically induced transparency," *Phys. Rev. Lett.* **64**(10), 1107–1110 (1990).
51. H. Schmidt and A. Imamoglu, "Giant Kerr nonlinearities obtained by electromagnetically induced transparency," *Opt. Lett.* **21**(23), 1936–1938 (1996).
52. S. E. Harris and L. V. Hau, "Nonlinear optics at low light levels," *Phys. Rev. Lett.* **82**(23), 4611–4614 (1999).
53. Y. Wu and X. Yang, "Highly efficient four-wave mixing in double- Λ system in ultraslow propagation regime," *Phys. Rev. A* **70**(5), 053818 (2004).
54. G. Wang, Y. Xue, J. H. Wu, Z. H. Kang, and J. Y. Gao, "Efficient frequency conversion induced by quantum constructive interference," *Opt. Lett.* **35**(22), 3778–3780 (2010).

55. C. K. Chiu, Y. H. Chen, Y. C. Chen, I. A. Yu, Y. C. Chen, and Y. Chen, "Low-light-level four-wave mixing by quantum interference," *Phys. Rev. A* **89**(2), 023839 (2014).
56. Z. Y. Liu, Y. H. Chen, Y. C. Chen, H. Y. Lo, P. J. Tsai, I. A. Yu, Y. C. Chen, and Y. Chen, "Large cross-phase modulations at the few-photon level," *Phys. Rev. Lett.* **117**(20), 203601 (2016).
57. D. A. Steck, "Rubidium 87 D line data," available online at <http://steck.us/alkalidata>.
58. K. Bergmann, H. Theuer, and B. W. Shore, "Coherent population transfer among quantum states of atoms and molecules," *Rev. Mod. Phys.* **70**(3), 1003–1025 (1998).
59. M. Scully and M. S. Zubairy, *Quantum Optics* (Cambridge University, Cambridge, 1997).
60. Y. Hong, L. Yang, X. C. Wang, C. L. Cui, and J. H. Wu, "Dynamically controlled two-color photonic band gaps via balanced four-wave mixing in one-dimensional cold atomic lattices," *Phys. Rev. A* **88**(6), 063832 (2013).
61. Y. Chen, P. Tsai, I. A. Yu, Y. Chen, and Y. Chen, "Phase-dependent double- Λ electromagnetically induced transparency," arXiv:1409.4153 (2014).
62. Y. F. Hsiao, H. S. Chen, P. J. Tsai, and Y. C. Chen, "Cold atomic media with ultrahigh optical depths," *Phys. Rev. A* **90**(5), 055401 (2014).
63. Y. Okamura, T. Negami, and S. Yamamoto, "Integrated optical isolator and circulator using nonreciprocal phase shifters: a proposal," *Appl. Opt.* **23**(11), 1886–1889 (1984).
64. P. Kok, W. J. Munro, K. Nemoto, T. C. Ralph, J. P. Dowling, and G. J. Milburn, "Linear optical quantum computing with photonic qubits," *Rev. Mod. Phys.* **79**(1), 135–174 (2007).